Capacitance Model of Embedded Transceiver for Intra-body Communication

Yuki Hayashida[1], Ryo Sugiyama[1], Yusuke Ido[1], Akito Suzuki[1], Yasuaki Takizawa[1], Mitsuru Shinagawa[1], Yuichi Kado[2], and Nozomi Haga[3]

[1]Faculty of Science and Engineering, Hosei University, 3-7-2, Kajino-cho, Koganei-shi, Tokyo, 184-8584, Japan

Phone: +81-42-387-6243

E-mail: yuki.hayashida.y8@stu.hosei.ac.jp

[2]Department of Electronics, Kyoto Institute of Technology, Matsugasaki, Sakyo-ku, Kyoto, 606-8585, Japan

[3]Faculty of Science and Technology, Gunma University, 1-5-1, Tenjin-cho, Kiryu-shi, Gunma, 376-8515, Japan

ABSTRACT

The transmission path of intra-body communication is composed of capacitance coupling among nodes. In this work, we used four nodes: body, signal and ground electrodes, and floor ground. It was reported that intra-body communication is affected by common-mode noise. As the impedance balance of the transmission path deteriorates, common-mode noise increases. The impedance elements can be replaced with the capacitance elements. We assumed approximate equations of capacitance elements and investigated them by changing the distance among the four nodes. We propose a 2-step procedure for estimating the equations of capacitance elements. It is confirm that the simulated results based on our model agree with the experimental results regarding common-mode noise, which validates the model.

Categories and Subject Descriptors

J.2 [**Computer Applications**]: PHYSICAL SCIENCES AND ENGINEERING– *Electronics, Engineering, Physics.*

General Terms

Measurement, Experimentation

Keywords

Intra-body communication, Capacitance measurement, Capacitance model, Common-mode noise.

1. INTRODUCTION

Intra-body communication [1] is a candidate for achieving ubiquitous computing [2]. A trigger of this communication system can be achieved through natural human action such as touching, sitting down, and walking.

BODYNETS 2014, September 29-October 01, London, Great Britain

DOI 10.4108/icst.bodynets.2014.258238

Therefore, it is a new type of communication that enables an intuitive interface to access a network and improves usability of communication [3].

This communication system treats a human body as a communication medium. Data are transmitted using the electric field from the surface of the human body. This system can be communicated through insulators such as clothes, shoes or bags. It is not necessary to touch the transceiver directly. Therefore intra-body communication is attracting attention as a communication technology for wide use, and various applications are expected [3].

When the electric field is used in the MHz band, it is regarded as quasi-electrostatic field [4]. Therefore, the surface of the human body is used as a transmission path and considered as a node [1]. Capacitance models around the human body have been reported [4-8].

Fig. 1 shows two types of transceivers for intra-body communication: wearable and embedded. [9-11].

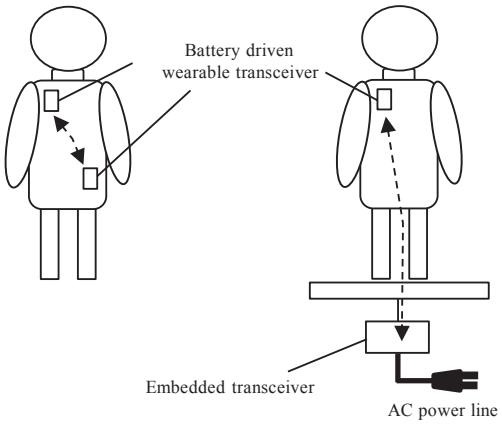

Fig. 1. Wearable and embedded transceivers.

Wearable transceivers are intended to be worn. Such transceivers are usually driven using a battery. There are many methods of wearing these transceivers: as a watch, headset or glasses. It is expected that the development of wearable transceivers in pursuit of design characteristics will advance.

Embedded transceivers are normally embedded in a floor, door, or table. These transceivers are driven using an AC power line. An example of communication between wearable transceivers has been reported [12,13]. There are many applications involving communication between wearable and embedded transceivers [9-11].

An authentication system using intra-body communication for a medical service is shown in Fig. 2. Data of a patient, such as personal, medical, and doctor information are transmitted to the hospital reception's PC by the patient just standing on a floor.

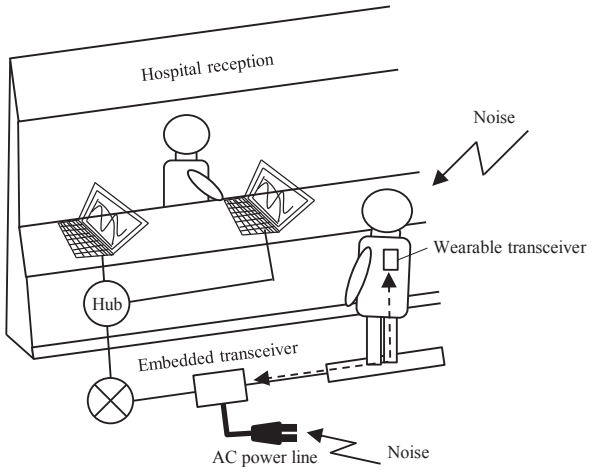

Fig. 2. Authentication system and medical service using intra-body communications in medical scene.

However, there is a serious problem with intra-body communication, i.e… common-mode noise [5,6]. Assuming a scene using an embedded transceiver, there are two types of common-mode noise. One is via floor ground (F-GND) in which the noise is transmitted through an AC power line. The other type of noise is via the body. The noise, from which electromagnetic waves a light or peripheral electronic equipment emits, is transmitted. These noises are transmitted as common-mode noise. It has been reported that an embedded transceiver is affected by such noise [5,6]. As the impedance balance of the transmission path deteriorates, common-mode noise increases [5,6]. The impedance elements can be replaced with the capacitance elements. Therefore, detailed study of the capacitance elements is required. We assumed the equations of capacitance elements and investigated them by changing the distance among four nodes. We confirm that the simulated results based on our model agree with the experimental results regarding common-mode noise.

2. CAPACITANCE MODEL

Fig. 3 shows the impedance model with a person standing on an embedded electrode for intra-body communication that was reported in a previous work [5]. The embedded electrode consists of a signal and a ground electrode to take the impedance matching of the transmission path. In our study, we considered four nodes: body, signal and ground electrodes, and F-GND.

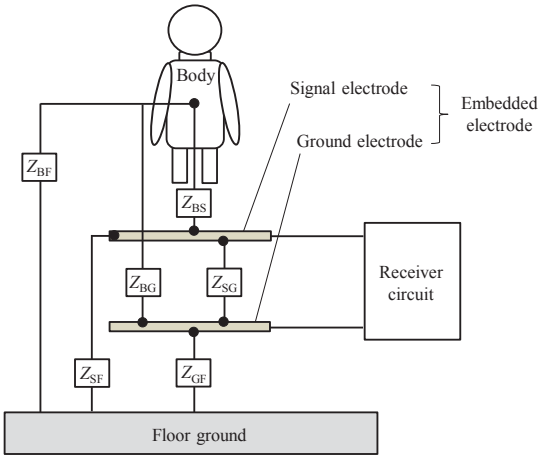

Fig. 3. Impedance model with body.

There are six impedance elements (Z_{BS}, Z_{BG}, Z_{BF}, Z_{SG}, $Z_{SF,}$ and Z_{GF}) among nodes. It has been reported that the impedance elements can be replaced with the capacitance elements [5]. Therefore, there are six capacitance elements (C_{BS}, C_{BG}, C_{BF}, C_{SG}, $C_{SF,}$ and C_{GF}). These elements depend on a person's actions, grounding condition, or state of the surrounding environment [14]. Fig. 4 shows the capacitance model [5].

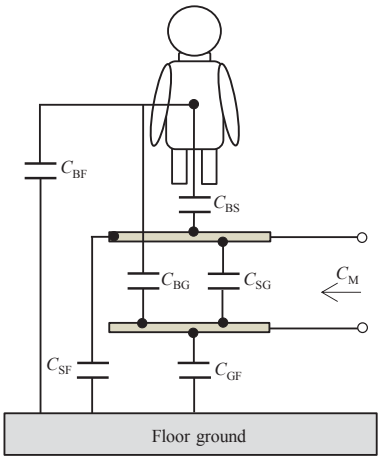

Fig. 4. Capacitance model with body.

The measured capacitance C_M between signal and ground electrodes is measured using a LCR meter. The measured capacitances without and with a body are C_{M0} and, $C_{MB,}$ respectively. Fig. 5 shows an equivalent circuit for the four nodes. Provided that C_{BS}, $C_{BG,}$ and C_{BF} are eliminated, C_{M0} is given by Eq. (1). This equivalent circuit is complicated for obtaining the C_{MB} equation. Δ-Y transformation is used for this equivalent circuit, as shown in Fig. 6 Three capacitance elements (C_{BFBG}, $C_{BFBS,}$ and C_{BGBS}) are given by Eqs. (2), (3), and (4), and C_{MB} i given by Eq. (5).

$$C_{M0} = C_{SG} + \frac{C_{SF} \times C_{GF}}{C_{SF} + C_{GF}} [F] \quad (1)$$

$$C_{BFBG} = \frac{C_{BF} \times C_{BG}}{C_{BF} + C_{BS} + C_{BG}} [F] \quad (2)$$

$$C_{BFBS} = \frac{C_{BF} \times C_{BS}}{C_{BF} + C_{BS} + C_{BG}} [F] \quad (3)$$

$$C_{BGBS} = \frac{C_{BG} \times C_{BS}}{C_{BF} + C_{BS} + C_{BG}} [F] \quad (4)$$

$$C_{MB} = \frac{(C_{SF} + C_{BFBS}) \times (C_{GF} + C_{BFBG})}{(C_{SF} + C_{BFBS}) + (C_{GF} + C_{BFBG})} + C_{BGBS} + C_{SG} [F] \quad (5)$$

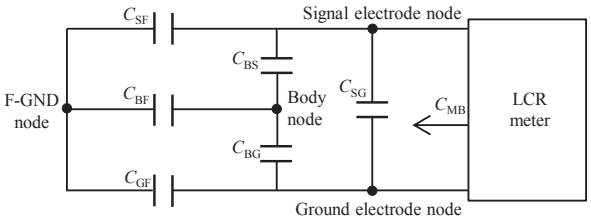

Fig. 5. Equivalent circuit on capacitance for four nodes: body,signal and ground electrodes, and F-GND.

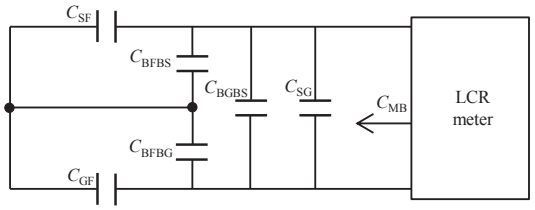

Fig. 6. Equivalent circuit on capacitance for four nodes after Δ-Y transformation.

3. MEASUREMENT SYSTEM

3.1 CAPACITANCE COUPLING WITH SURROUNDING ENVIRONMENT

Before measuring capacitance elements in the model, the surrounding environment must be considered [14]. Fig. 7 shows a measurement system for capacitance coupling strength between the measuring instrument and F-GND. A LCR meter (Agilent U1733) is used for measuring capacitance elements.

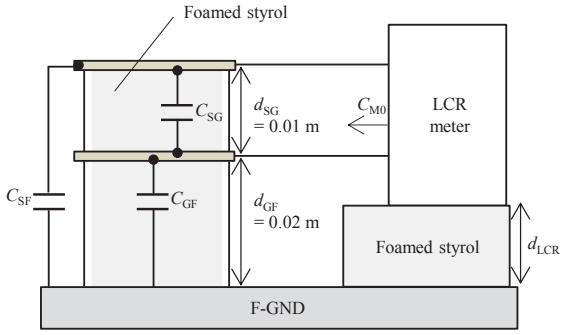

Fig. 7. Measurement system for capacitance coupling strength between the measuring instrument and F-GND.

There are two kinds of experimental methods for investigating the capacitance coupling strength between the LCR meter and F-GND. The distance d_{LCR}, d_{SG} and d_{GF} are defined by sandwiching foamed styrol as insulation plates. One method involves changing d_{LCR} by changing the thickness of the foamed styrol. The other involves changing d_{LCR} by floating with hand. The d_{SG} and d_{GF} are fixed 0.01 m and 0.02 m respectively. It is investigated that the changed by changing d_{LCR} with these methods. Fig. 8 shows the d_{LCR} dependence of measurement system.

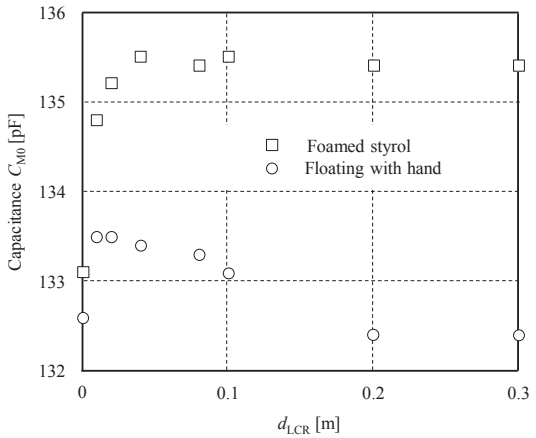

Fig. 8. d_{LCR} dependence of measurement system.

When d_{LCR} is less than 0.1 m, both methods exhibit the d_{LCR} dependence. When d_{LCR} is more than 0.2 m and the human body has the LCR meter, C_{M0} decreases. It is considered that there is capacitance coupling with F-GND through the human body. However, when the human body doesn't have the LCR meter, C_{M0} is constant since capacitance coupling with F-GND is weak. Therefore, to reduce capacitance coupling with F-GND and a body, we set the LCR meter to 0.2 m from F-GND.

Fig. 9 shows the measurement system for capacitance coupling strength between electrodes and F-GND: ceiling or floor. Fig. 10 shows the d_{GF} dependence of C_{M0} without a body.

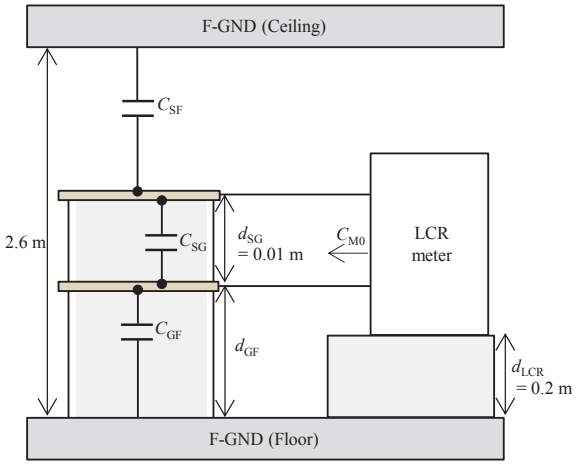

Fig. 9. Measurement system for capacitance coupling strength between electrodes and F-GND: Ceiling or Floor.

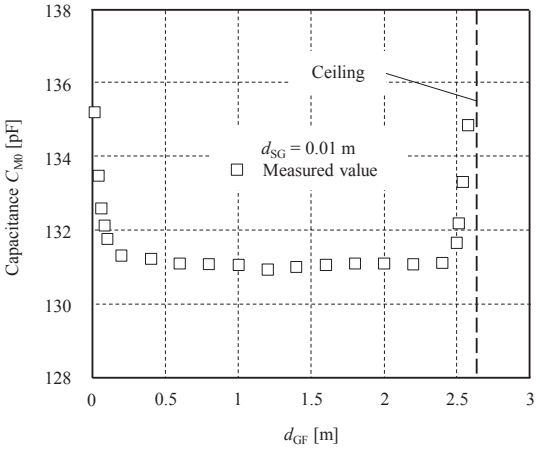

Fig. 10. The d_{GF} dependence of capacitance C_{M0} without body.

The distance from the floor to a ceiling was approximately 2.6 m in the laboratory. When d_{SG} was 0.01 m and d_{GF} changed by changing the thickness of the foamed styrol from 0.02 to 2.56 m, C_{M0} was measured.

As shown in Fig. 10, when d_{GF} was less than 0.2 m and more than 2.4 m, capacitance coupling with F-GND was strong. Therefore, not only capacitance coupling strength with the floor, but also with the ceiling must be considered. To reduce capacitance coupling with the ceiling, we set the height from the floor in the measurement system to 2.4 m.

3.2 ESTIMATION PROCEDURE OF CAPACITANCE ELEMENTS

Fig. 11 shows the measurement system for capacitance elements. The d_{BS}, $d_{SG,}$ and d_{GF} are defined by sandwiching foamed styrol as insulation plates between the four nodes. Fig. 12 shows a photograph of the experimental setup for capacitance measurement with a body. The electrodes are signal and ground electrodes, of 365 × 365 × 0.3 mm. The d_{BS}, d_{SG} and d_{GF} can be changed by changing the thickness of the foamed styrol. The C_{M0} and C_{MB} are measured using a LCR meter at a test signal frequency of 100 kHz.

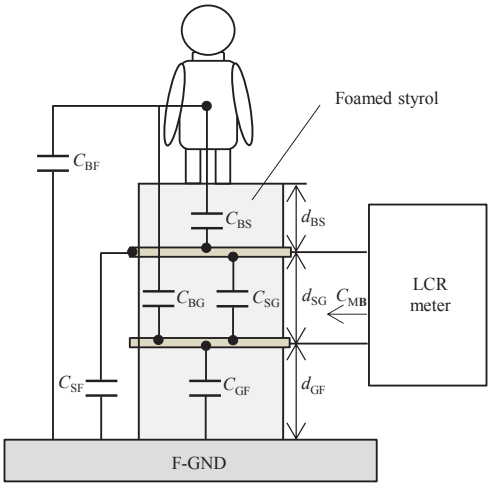

Fig. 11. Measurement system for capacitance elements.

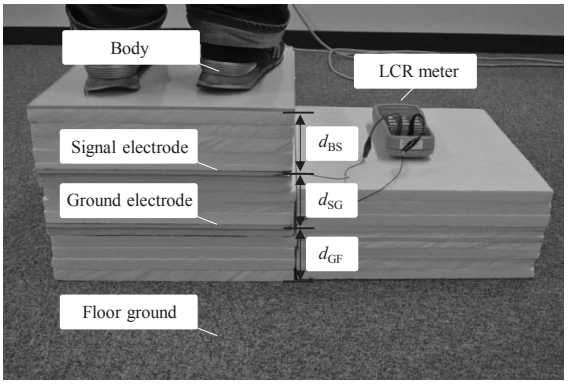

Fig. 12. Photograph of experimental setup for capacitance measurement with body.

We propose a 2-step procedure for estimating the equations of six capacitance elements in the model shown in Fig. 11. The procedure is summarized in Table 1. The first step is an experimental setup using two electrodes without a body. The d_{SG} and d_{GF} are changed to estimate C_{SG}, $C_{SF,}$ and C_{GF}. The second step is an experimental setup using two electrodes with a body. The distances d_{BS}, d_{SG} and d_{GF} are changed to estimate C_{BS}, $C_{BG,}$ and C_{BF}. The capacitance of the parallel conductor is proportional to distance d^{-1} among the nodes. Therefore, capacitance element, C is given by Eq. (7).

$$C = \alpha \times d^{-\beta} + C_0[\mathrm{F}] \quad (7)$$

Where d is the distance among nodes, α and β are the functions of the decrement depending on the shape and size of the conductor, and C_0 is the background capacitance of the measurement system. These variables are determined by fitting the experimental curve. It refers same α and β for the equations of C_{SF} and $C_{GF,}$ and α and β for the equations of C_{BS} and C_{BG}.

Table 1
Procedure to estimate capacitance elements.

	First step	Second step
Experimental setup :Two electrodes	Without body	With body
Change the distance	d_{SG},d_{GF}	d_{BS},d_{SG},d_{GF}
Elements estimated	C_{SG}	C_{BS}
	C_{SF}	C_{BG}
	C_{GF}	C_{BF}

4. EXPERIMENTAL RESULTS

Fig. 13 shows the d_{SG} and d_{GF} dependence of C_{M0}. In the first step, C_0 was determined as 1.7 pF from the experiment with only the measurement system. When d_{GF} was large enough to ignore the second term of Eq. (1), α and β for the $C_{SG,}$ equation was determined by fitting the experimental curve for changing d_{SG}. When d_{SG} was 0.01 m, α and β for C_{SF} and C_{GF} equations were determined by fitting the experimental curve for changing d_{GF}. The calculated values were given by substituting the equations of C_{SG}, C_{SF} and C_{GF} into Eq. (1). Fig. 14 shows the d_{BS}, d_{SG} and d_{GF} dependence of C_{MB}. As shown in Fig. 15, C_{BF} had little effect on C_{MB}. Therefore, it was assumed that C_{BF} was 110 pF, as reported by Zimmerman [1]. In the second step, α and β for the C_{BS} and C_{BG} equations, except for $C_{BF,}$ were determined by fitting the experimental curve for changing d_{BS}, d_{SG} and d_{GF}. The calculated values were given by substituting the C_{BS}, C_{BG} and C_{BF} equations into Eqs. (2), (3), (4), and (5), respectively. The equations of capacitance elements are summarized in Table 2.

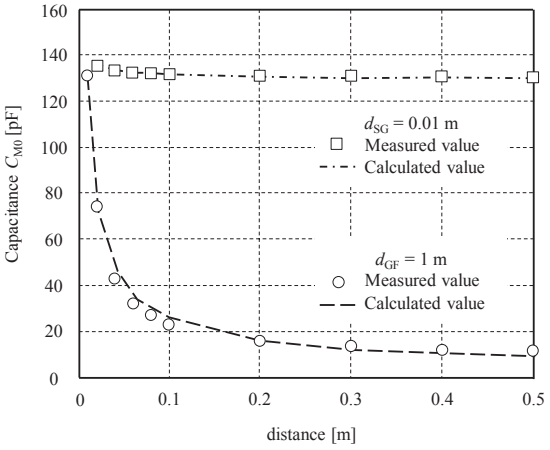

Fig. 13. Distance dependence of capacitance C_{M0} without body.

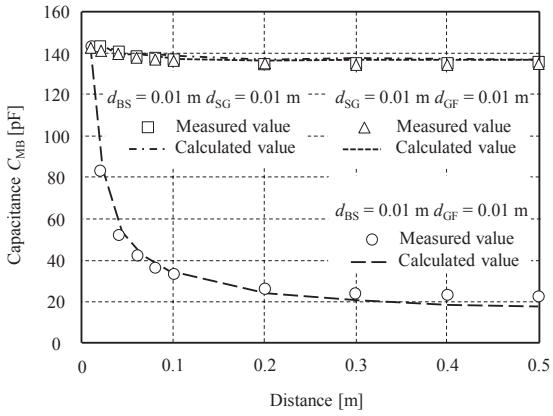

Fig. 14. Distance dependence of capacitance C_{MB} with body.

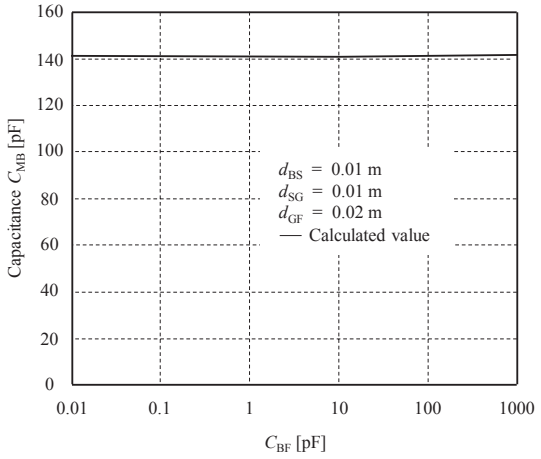

Fig. 15. Capacitance C_{BF} dependence of capacitance C_{MB}.

Table 2
Approximated equation of capacitance elements.

Capacitance elements	Approximated equation
C_{SG}	$4.6*d_{SG}^{-0.72}+1.7$
C_{SF}	$1.7*d_{SF}^{-0.52}+1.7$
C_{GF}	$1.7*d_{GF}^{-0.52}+1.7$
C_{BS}	$0.9*d_{BS}^{-0.6}+1.7$
C_{BG}	$0.9*d_{BG}^{-0.6}+1.7$

Fig. 16 shows a basic model of common-mode and differential-mode noise on the transmission path of intra-body communication [5]. The signal amplitude V_{SIG} is input to the receiver circuit via the transmission path: a signal and a circuit ground path.

The term Z_1 is the signal path impedance, Z_2 is the circuit ground path impedance, Z_3 is the parasitic impedance between the signal path and ground, and Z_4 is the parasitic impedance between the circuit ground and ground.

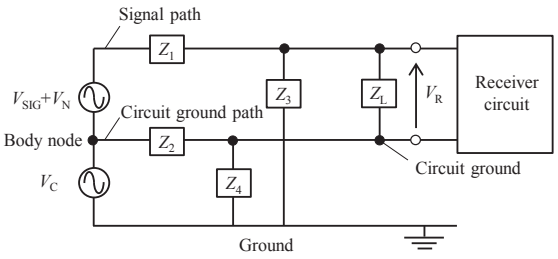

Fig. 16. Basic model of common-mode and differential-mode noise on transmission path in the intra-body communications.

Generally, there are two types of noise via the transmission path: differential-mode noise V_N and common-mode noise V_C [15,16]. The V_N arises between the signal path and circuit ground path. It is transmitted as the same path as V_{SIG}. The V_C arises between the signal path, the circuit ground path and ground. It is transmitted in the same direction in the transmission path and returned via the ground as a return path.

When V_R is the received voltage, V_C is given by Eq. (8). As the impedance balance of the transmission path deteriorates, V_C increases [5]. This causes noise interference to remote electronic equipment, and canceling such noise is difficult.

$$V_R = V_C\left(\frac{Z_3}{Z_1+Z_3}-\frac{Z_4}{Z_2+Z_4}\right) \quad (8)$$

Fig. 17 shows a noise model of the transmission path [5]. The F-GND and power source ground (P-GND) are distinct from Earth ground (E-GND), since the electrical property that each ground has is unknown. The impedance between F-GND and P-GND is Z_{FP} and the capacitance between a body and E-GND is 1 pF. There are two types of common-mode noise: V_{CNF} and V_{CNB}. The V_{CNF} is via F-GND and, is transmitted through an AC power line, and V_{CNB} is via the body. The noise, from which electromagnetic waves that a light or peripheral electronic equipment emits, is transmitted. In this work, V_{CNB} was added to previously proposed model.

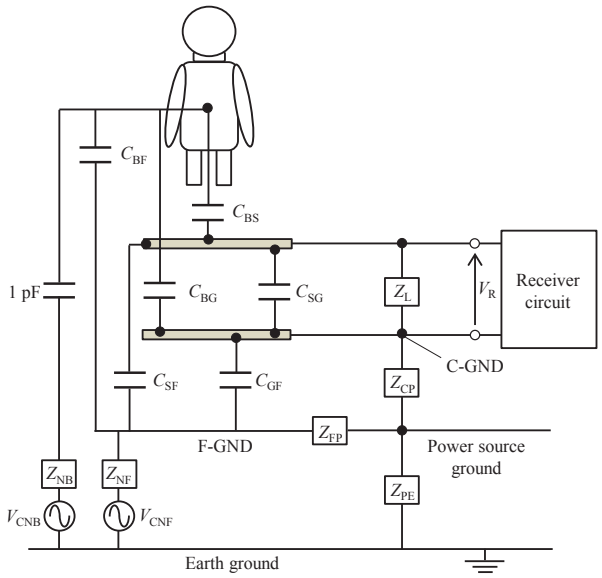

Fig. 17. Noise model of transmission path.

The common-mode rejection ratio (*CMRR*) [17] to express how much noise can be eliminated was used. As *CMRR* becomes large, common-mode noise can be eliminated. When V_{CNF} and V_{CNB} are expressed by V_{CN} and the load impedance Z_L is large, the *CMRR* can be given by Eq. (9).

$$CMRR = 20\log\left(\frac{V_{CN}}{V_R}\right)[\mathrm{dB}] \quad (9)$$

There are two types of simulation methods: that involving V_{CNF} and that involving V_{CNB}. Fig. 18 shows the d_{BS} dependence of the *CMRR* obtained from the simulated results using Eq. (9). The d_{BS} was between 0.01 and 0.1 m, and V_{CNF} changes little. However, V_{CNB} affected the body. Its difference was about 8 dB. We confirm that the simulated results based on our model agree with the experimental results reported in a previous work [4] regarding common-mode noise, which validates the model. In our laboratory environment, the main common-mode noise was via the body.

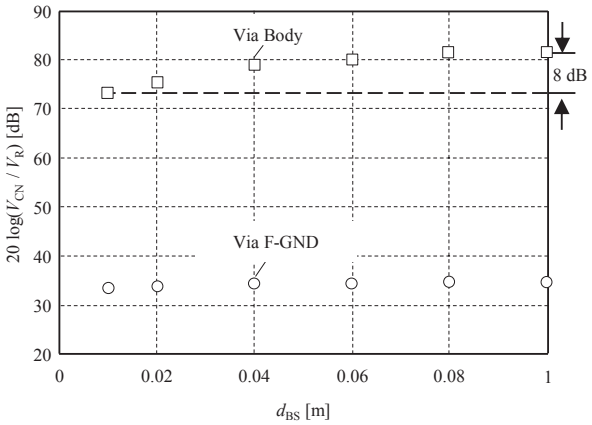

Fig. 18. d_{BS} dependence of *CMRR*.

5. CONCLUSION

The transmission path of intra-body communication is composed of the parasitic capacitances among nodes. We assumed approximate equations of capacitance elements and investigated them by changing the distance among four nodes. We confirm that the simulated results based on our model agree with the experimental results regarding common-mode noise. Therefore, our model is valid.

6. ACKNOWLEDGEMENTS

The authors would like to thank Jun Katsuyama, Kazuki Matsumoto, Hiroyuki Hatanaka and Yoko Yabe for their advice and, help with the experiments.

7. REFERENCES

[1] T. G. Zimmerman. 1996. Personal Area Networks: Near-field intrabody communication. *IBM System.* J, 35 (3/4) 609-617.

[2] M. Weiser. 1991. The computer for the twenty-first century. *Scientific Amer.* 265, 94-103.

[3] Y. Kado and M. Shinagawa. 2010. AC Electric Field Communication for Human-Area Networking. *IEICE Trans. Electron.* E93-C, No. 3, 234-243.

[4] N. Haga, K. Saito, M. Takahashi, and K. Ito. 2012. Proper Derivation of Equivalent-Circuit Expressions of Intra-Body

Communication Channels Using Quasi-Static Field. *IEICE Trans. Commun.* E95-B, No. 1, 51-59.

[5] M. Shinagawa, J. Katsuyama, K. Matsumoto, S. Hasegawa, R. Sugiyama and Y. Kado. 2014. Noise analysis for intra-body communication based on parasitic capacitance measurement. *Elsevier Measurement 51.* 206-213.

[6] A. Sasaki, T. Ishihara, N. Shibata, R. Kawano, H. Morimura, and M. Shinagawa. 2013. Signal-to-Noise Ratio Analysis of a Noisy-Channel Model for a Capacitively Coupled Personal Area Network. *IEEE Trans. Antennas Propag*. 61, No. 1, 390-402.

[7] R. Sugiyama, Y. Hayashida, J. Katsuyama, K. Matsumoto, Y. Ido, M. Shinagawa and Y. Kado. 2013. Signal Analysis of Wearable Transmitter for Intra-body Communication. *BodyNets. ICST* 449-452.

[8] T. Minotani and M. Shinagawa. 2014. Methods of Estimating Return-Path Capacitance in Electric-Field Intrabody Communication. *IEICE Trans. Commun.* E97-B, No. 1, 114-121.

[9] Y. Kado, T. Kobase, T. Yanagawa, T. Kusunoki, M. Takahashi, R. Nagai, O. Hiromitsu, A. Hataya, H. Shimasaki, and M. Shinagawa. 2012. Human-Area Networking Technology Based on Near-Field Coupling Transceiver. *2012 IEEE Radio & Wireless Sym. (RWS 2012),* p119-122.

[10] R. Nagai, T. Kobase, T. Kusunoki, H. Shimasaki, Y. Kado and M. Shinagawa. 2012. Near-Field Coupling Communication Technology For Human-Area Networking. *Journal of Systemics, Cybermetics & Informatics, Vol. 10, Issue 6,* p14.

[11] M. Nozawa, T. Nakamura, H. Simasaki, Y. Kado and M. Shinagawa. 2013. Signal Measurement System Using Electrically Isolated Probe for MHz-Band Near-Field Coupling Communication. *IEEE International Instrumentation and Measurement Technology Conference 2013*, 37-40.

[12] M. Ishida, T. Nakamura, M. Nozawa, N. Watanabe, Y. Kado, and M. Shinagawa. 2014. MHz-Band RF Signal Propagation Characteristics on Human Body for Intra-body communication. *IEEE International Instrumentation and Measurement Technology Conference 2014*, p797-801.

[13] M. Ishida, T. Nakamura, M. Nozawa, N. Watanabe, H. Shimasaki, Y. Kado, and M. Shinagawa. Signal Propagation Characteristics between Transceivers on Human Body for Mhz-Band Near-field Coupling Communication. *8th international Conference on body area networks*, 453-456.

[14] R. Xu, W. C. Ng, H. Zhu, H. Shan and J. Yuan. 2012. Equation Environment Coupling and Interference on the Electric-Field Intrabody Communication Channel. *IEEE Trans. Biomedical Engineering,* 59, No.7, 2051-2059

[15] Daniel Cochrane, Dan Y. Chen and Dushan Boroyevic. 2003. Passive Cancellation of Common-Mode Noise in Power electronic Circuits. *IEEE Trans On Power Electronics* Vol. 18, No. 3, 756-763.

[16] T. Guo, D Y. Chen and F C. Lee. 1996. Separation of the Common-Mode- and Differential-Mode-Conducted EMI Noise. *IEEE Trans On Power Electronics*. Vol. 11, No. 3, 480-488.

[17] J. Zhou and J. Liu. 2005. On the Measurement of Common-Mode Rejection Ratio. *IEEE Trans. Circuits and Systems.* 52, No.1, 49-53.